Mesoporous Materials

Single-Crystal Mesoporous Silica Ribbons**

*Jianfang Wang, Chia-Kuang Tsung, Ryan C. Hayward, Yiying Wu, and Galen D. Stucky**

Mesoporous materials have many present and potential future applications for catalysis, chemical and biological separations, chromatography, photonic and electronic devices, drug delivery, and energy storage.[1] They are typically synthesized with amphiphilic organic molecules as templates through the cooperative assembly between these molecules and inorganic species. Since their discovery, control of ordered mesoporous structures and pore sizes has been widely investigated by changing synthetic conditions and by using different types of amphiphiles, including small charged surfactant molecules and large block copolymers. Meanwhile, progress has also been made in the assembly of surfactant molecules and inorganic species into mesoporous materials with a wealth of morphological shapes and internal pore architectures, such as spheres,[2] gyroids,[3] fibers,[4–6] tubules,[7] and thin films,[8] for a variety of applications. Furthermore, cooperative assembly between inorganic and organic components has recently become an exciting approach for the development of novel multifunctional materials.[9]

Ribbon-shaped one-dimensional nanostructures made of transition metals,[10] transition metal oxides,[11] and II–VI semiconductor compounds[12] have been extensively investigated owing to their distinctive geometries, novel physical and chemical properties, and potential applications in magnetic, electronic, and photonic devices. These inorganic ribbons are prepared by using either a vapor–solid or a solution–solid process. They exhibit the same crystallographic structures as the corresponding bulk materials and are usually enclosed by low-index facets with rectangular cross sections. Here, we report the synthesis of single-crystal mesoporous silica ribbons by using small cationic surfactant molecules. These ribbons have tracklike pore channels that are oriented perpendicular to the length of the ribbon and are hexagonally

[*] Dr. J. Wang, C.-K. Tsung, Dr. Y. Wu, Prof. G. D. Stucky
Mitsubishi Chemical Center for Advanced Materials
Department of Chemistry and Biochemistry
University of California
Santa Barbara, CA 93106 (USA)
Fax: (+1) 805-893-4120
E-mail: stucky@chem.ucsb.edu

R. C. Hayward
Department of Chemical Engineering
University of California
Santa Barbara, CA 93106 (USA)

[**] This work was supported by Mitsubishi Chemical Center for Advanced Materials, the National Science Foundation (award No. DMR 01-20967), and an IBM faculty award to G. D. Stucky and made use of MRL Central Facilities supported by the MRSEC Program of the National Science Foundation (award No. DMR 00-80034). We gratefully acknowledge the assistance provided by Peter Allen in the artistic illustration of the internal pore architecture of the mesoporous ribbons.

  DOI: 10.1002/ange.200461296

packed together. The internal pore architecture of these ribbons is significantly different from the two-dimensional hexagonal mesostructure. Previously, helically twisted silica ribbons were prepared with a chiral phospholipid, but they have a lamellar mesostructure that collapses upon calcination.[13] Furthermore, silica ribbons with hexagonal mesoporous structures have been prepared with electrospinning, but the organization of their pore channels is polycrystal-like with the pore channels in different domains oriented randomly.[14] To the best of our knowledge, there have been no reports on the formation of single-crystal-like mesostructured silica ribbons with highly organized pore channels remaining after calcination.

In the past, a two-phase route has been used to synthesize one-dimensional mesostructured silica materials with silica precursor molecules dissolved in an oil phase and surfactant molecules dissolved in a separate water phase.[4,15] The morphologies and internal pore architectures of the resulting mesostructured products depend strongly on the supply of silica precursor molecules that diffuse from the oil phase through the interface to the water phase.

In contrast, we believe that a one-phase synthesis procedure carried out in dilute aqueous solutions of surfactant molecules and hydrolyzed silica species might be used to reduce the nucleation and growth rates of mesostructured products. By this procedure, their morphological shapes and internal pore architectures would be largely determined by the cooperative assembly between silica species and surfactant molecules in a single aqueous growth solution. With this in mind, we have developed a one-phase route to synthesize one-dimensional mesostructured silica materials with cationic hexadecyltrimethylammonium or hexadecylpyridinium surfactants as templates and tetraethyl orthosilicate (TEOS) as a silica precursor under acidic conditions. This approach has been used to selectively synthesize either mesostructured silica nanofibers that have hexagonal fiber cross sections with pore channels aligned parallel to the fiber axis or mesostructured silica fibers that have circular fiber cross sections with pore channels wound circularly around the fiber axis with an acid concentration of approximately 4.0 M.[6] The one-phase route can readily expand the kinetic control range of synthetic parameters, including the concentration of the acid, temperature, concentrations of the surfactant and the silica precursor, and the type of surfactant, and it has the potential to allow the synthesis of more complicated mesostructured configurations. Indeed, we found that the one-phase synthesis with an acid concentration in the range of 1.0–2.0 M led to the formation of one-dimensional mesostructured silica materials that were all in the form of ribbons.

After the one-phase synthesis, fiberlike flocculates were seen suspended in the growth solutions. Scanning electron microscopy (SEM) images taken of the flocculates, which were isolated, washed with distilled water, and dried, indicate that they consist of a large quantity of fiberlike structures with typical lengths of the order of several hundreds of micrometers (Figure 1a). SEM imaging at higher magnifications reveals that the geometrical shape of the silica fiberlike structures is a ribbon (Figure 1a, inset), which is clearly distinct from the shape of the previously reported mesostructured fibers.[4–6] Each silica ribbon has a relatively uniform width along its entire length, and the typical widths of the ribbons are in the range of 0.4–1.5 μm. Some ribbons were seen twisted along both their length and width axes, which suggests that as-synthesized mesostructured silica ribbons have a low bending stiffness. Low-angle X-ray diffraction (XRD) measurements show that the as-synthesized ribbon sample exhibits two diffraction peaks, which remain after calcination (Figure 1b), indicating that these ribbons are ordered mesostructures. The diffraction patterns can be indexed according to a two-dimensional hexagonal lattice. The determined lattice constant for the as-synthesized ribbons is $a = 4.7$ nm, which reduces to $a = 4.3$ nm after calcination.

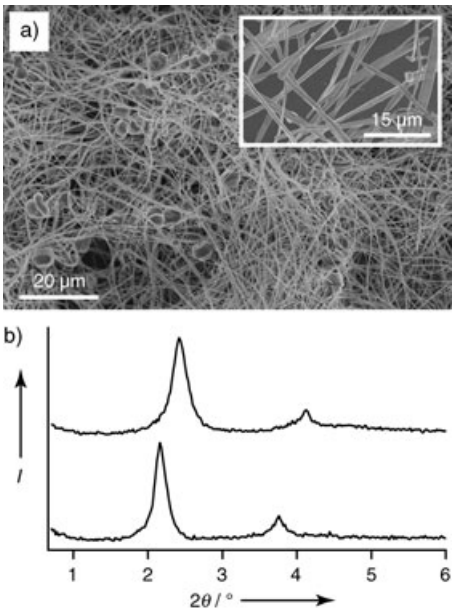

Figure 1. Mesoporous silica ribbons. a) SEM image of the mesostructured ribbons synthesized with hexadecylpyridinium bromide (C_{16}PB) surfactant. Inset: a magnified SEM image showing clearly the ribbon shape of the synthesized products. b) Low-angle XRD patterns recorded on the as-synthesized (lower; $d(100) = 4.09$ nm, $d(110) = 2.35$ nm, $a = 4.7$ nm) and calcined (upper; $d(100) = 3.65$ nm, $d(110) = 2.15$ nm, $a = 4.3$ nm) ribbons.

Low-magnification transmission electron microscopy (TEM) images confirm that the geometrical shape of the fiberlike structures is a ribbon (Figure 2a) and that each ribbon has a uniform width along its length (Figure 2b). From the TEM images taken at high magnifications of the individual ribbons that are flat and straight, hexagonally packed pore channels are observed at the edge of each ribbon, whereas parallel fringes oriented perpendicular to the length of the ribbon are observed in the central region of the ribbon (Figure 2c). In fact, the hexagonally packed pore channels are visible at both the left and right edges of each ribbon. Moreover, the hexagonally packed pore channels at the edges and the parallel fringes in the central region can be seen over the entire length of the individual ribbons that are straight and untwisted, which demonstrates that these ribbons are structurally uniform.

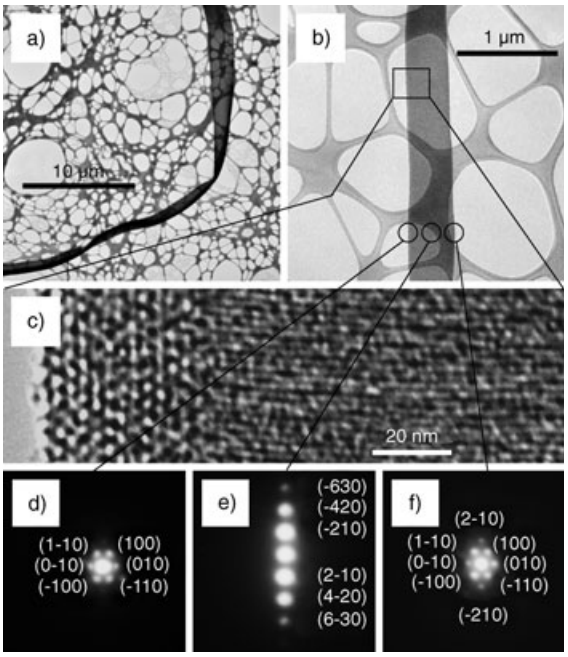

Figure 2. TEM images of mesoporous silica ribbons showing their geometrical shape and internal pore architecture. The ribbons were synthesized with C_{16}PB surfactant and calcined. a) TEM image of a twisted ribbon that shows the characteristic ribbon shape. b) TEM image of a straight ribbon that shows a uniform width along its length. c) Zoomed-in TEM image of the boxed area in Figure 2b that shows hexagonally packed pore channels at the edge and parallel fringes oriented perpendicular to the length of the ribbon in the central region of the ribbon. d)–f) Selected-area electron diffraction patterns taken at the left edge, in the central region, and at the right edge, respectively, of the ribbon shown in Figure 2b. The diffraction patterns are indexed according to a two-dimensional hexagonal lattice. The zone axes for Figure 2, d–f, are [001], [120], and [001], respectively.

The organization of the pore channels in the mesoporous silica ribbons is also revealed by the selected-area electron diffraction patterns recorded at the edges and in the central region of the individual ribbons. Hexagonal diffraction patterns are observed at the edges (Figure 2, d and f) and a string of diffraction spots are obtained in the central region (Figure 2e) which indicates that each mesoporous ribbon is single-crystalline. The diffraction patterns recorded at the edges and in the central region can be indexed separately according to a two-dimensional hexagonal lattice, with zone axes [001] and [120], respectively.

To further verify the morphological characteristics and ascertain the internal pore architecture of the mesoporous silica ribbons, we performed microtoming to cut thin cross-sectional slices of the ribbons. Figure 3, a and c show the TEM images of the cross sections that are perpendicular to the length of the ribbon. These cross sections are semicircular at the edges and rectangular in the central region. The cross-sectional TEM images at higher magnifications reveal that the pore channels in the central region are aligned parallel to the width of the ribbon (Figure 3b) and those at the edges curve around semicircularly (Figure 3d). These pore channels appear to be tracklike, and the curvatures of the pore channels from outside to inside at the edges become increasingly larger. The pore channels that are close to the central region curve back to make sharp turns of 180° and the innermost channel becomes a single straight pore channel. Furthermore, we also observed cross sections that are parallel to the length of the ribbon (Figure 3, e and f) as judged on the basis of the cross-sectional size and the organization of the pore channels. With this viewing configuration, hexagonally packed pore channels aligned parallel to the width of the ribbon are observed.

Taking together all of the structural observations of the mesoporous ribbons, including selected-area electron diffraction patterns and high-magnification TEM images recorded from different viewing directions, we have constructed a three-dimensional model of the internal pore architecture of the mesoporous silica ribbons (Figure 4). Each ribbon is composed of a large number of tracklike pore channels that are oriented perpendicular to the length of the ribbon and are hexagonally packed together. For a ribbon with a thickness of 120 nm, a width of 800 nm, and a length of 100 μm, which are the typical dimensions of these mesoporous ribbons, it is estimated that there are about 4×10^5 tracklike pore channels with perimeters in the range of 1 to 2 μm. It is remarkable that such a large number of the pore channels with a uniform pore size and varying perimeters can assemble together with such high order to form a mesoporous ribbon.

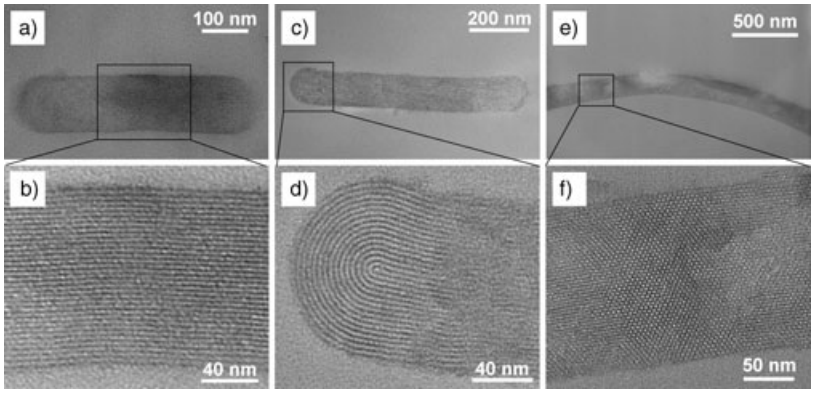

Figure 3. Cross-sectional TEM images of mesoporous silica ribbons showing their geometrical shape and internal pore architecture. The ribbons were synthesized with C_{16}PB surfactant and calcined. a) TEM image of a cross section that is perpendicular to the length of the ribbon. The ribbon has a width-to-thickness ratio of approximately 4.3. b) Zoomed-in TEM image of the boxed area in Figure 3a that shows parallel pore channels in the central region of the ribbon. c) TEM image of a cross section that is perpendicular to the length of the ribbon. The ribbon has a width-to-thickness ratio of about 7.0. d) Zoomed-in TEM image of the boxed area in Figure 3c that shows pore channels curving back at the edge of the ribbon. e) TEM image of a cross section that is parallel to the length of the ribbon. Only a short segment is shown here: the actual length of the ribbon is more than 10 μm. f) Zoomed-in TEM image of the boxed area in Figure 3e that shows hexagonally packed pore channels. The occurrence of blurred lattice structures in some regions of the ribbons is probably due to the nonuniform distribution of strain induced by microtoming.

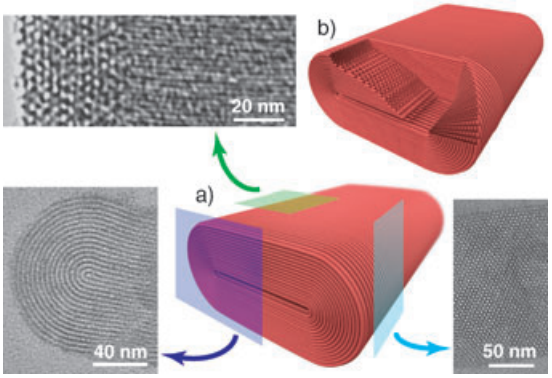

Figure 4. Three-dimensional model of the pore structure of individual mesoporous silica ribbons. a) Overview with overlapping planes showing the relationship between recorded TEM images and different viewing directions relative to the ribbon. b) A portion is cut away to show the internal pore architecture.

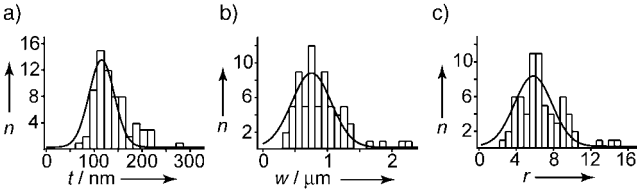

Figure 5. Size distributions of the calcined mesoporous silica ribbons synthesized with C_{16}PB surfactant: a) thickness (t), b) width (w), and c) width-to-thickness ratio (r). The number of counted ribbons is 68.

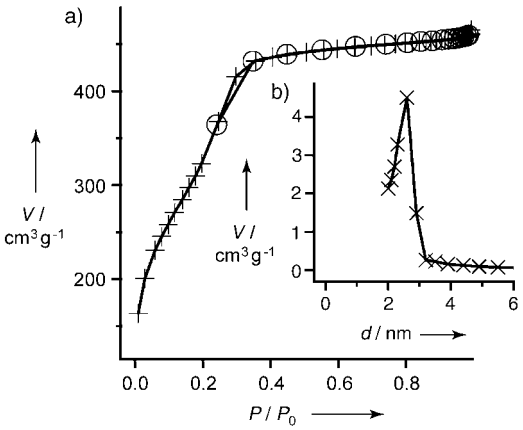

Figure 6. Nitrogen adsorption–desorption measurements of mesoporous silica ribbons obtained with C_{16}PB surfactant. a) Sorption isotherms (+ = adsorption, ○ = desorption). b) BJH pore size distribution obtained from the adsorption branch (d = diameter).

According to the three-dimensional model, hexagonally packed pore channels at the edges and parallel fringes in the central region are visible under TEM imaging when a mesoporous ribbon that stays flat and straight is viewed normal to its flat portion. The top and bottom surfaces of the flat portion of the ribbon are enclosed by ±(010) facets. On the basis of the organization of the pore channels as shown in Figure 4, the spacing between the neighboring parallel fringes in the central region should be half of the hexagonal lattice constant at the edges, which is in excellent agreement with the measurements made by using the TEM images as shown in Figure 2c. Furthermore, it can be seen from the model that tracklike pore channels are visible on the cross sections that are perpendicular to the length of the ribbon, and hexagonally packed pore channels are visible on the cross sections that are parallel to the length of the ribbon, which is also in agreement with our observations from TEM.

The internal pore architecture of the mesoporous silica ribbons is not a simple truncation of the two-dimensional hexagonal mesostructure. As described above, the pore channels in the mesoporous ribbons are curved at the edges with a tracklike conformation. Unlike the transition metal oxide ribbons, which are enclosed by low-index facets and have rectangular cross sections,[11] the mesoporous silica ribbons have smooth external surfaces without sharp edges. There have been no reported materials that exhibit such structures. The closest structural analogy are ribbons obtained from the spontaneous hierarchical self-assembly of highly charged cytoskeletal filamentous actin and cationic lipid membranes.[16] These ribbons also exhibit tracklike cross sections, but are composed of folded two-dimensional lipid bilayers sandwiched between two layers of actin.

The size distributions of the mesoporous silica ribbons were measured from the cross-sectional TEM images taken on microtomed samples (Figure 5). The ribbons have an average thickness of (120 ± 30) nm, an average width of (0.8 ± 0.3) μm, and an average width-to-thickness ratio of (6 ± 2).

The nitrogen adsorption–desorption isotherms measured at −196 °C for the calcined mesoporous silica ribbons are shown in Figure 6a. The isotherms can be classified as type IV isotherms without hysteresis. The ribbons exhibit a nitrogen Brunauer–Emmett–Teller (BET) surface area of 1200 $m^2 g^{-1}$, and the single-point total desorption pore volume at a relative pressure of 0.98 is 0.71 $cm^3 g^{-1}$. The Barrett–Joyner–Halenda (BJH) pore size distribution plot (Figure 6b) determined from the adsorption branch shows a sharp peak at 2.6 nm with a full width at half maximum (FWHM) of 0.8 nm.

In summary, single-crystal mesoporous silica ribbons that are 50–250 nm thick, 0.4–1.5 μm wide, and hundreds of micrometers long have been synthesized by using a one-phase route in dilute aqueous solutions of surfactants and silica species under acidic conditions. The mesoporous ribbons have excellent long-range order with tracklike pore channels oriented perpendicular to the length of the ribbon and hexagonally organized. Our one-phase route to the selective synthesis of one-dimensional mesostructured silica ribbons, together with our previously reported mesostructured silica nanofibers with controlled cross-sectional shapes and internal pore architectures,[6] provides a relatively simple reaction system for further developing theoretical models for the cooperative assembly between inorganic and organic components. Understanding the thermodynamics and growth kinetics involved in the formation of the mesostructured materials of particular morphological shapes and internal pore architectures can further help in creating novel inorganic–organic hybrid functional materials with desired hierarchical structures through the cooperative assembly between inorganic and organic building components.[9]

Experimental Section

Mesostructured silica ribbons were prepared with cationic hexadecyltrimethylammonium or hexadecylpyridinium surfactants and TEOS (tetraethyl orthosilicate) silica precursor. In a typical synthesis batch with C_{16}PB (hexadecylpyridinium bromide) surfactant, a 37 wt% solution of HCl (6.51 g) was mixed with distilled water (43.49 g), and C_{16}PB (0.21 g) was dissolved into this mixture. The resulting solution was stirred until the surfactant molecules were dissolved completely. TEOS (177 μL) was then added. After the solution was stirred at room temperature for 10 min, it was transferred to a 60 mL glass vessel. The vessel was closed and kept in an isothermal oven at approximately 65 °C for 2 days. Within this period of time, fiberlike flocculates suspended in the solution were observed. The flocculates were removed after growth, washed with distilled water, and dried at 100 °C in air. The yield of mesostructured ribbons from each synthesis was estimated to be about 25 wt%. To remove cationic surfactants, dried ribbon samples were calcined in a box furnace in air at 500 °C for 5 h, with a ramp rate of 1 °C min^{-1}. We found that mesostructured silica ribbons can only be synthesized within a certain range of concentration of HCl. The reaction composition with which ribbons can be obtained for C_{16}PB is 100 H_2O:2.0–3.5 HCl:0.02 C_{16}PB:0.03 TEOS (in molar ratio). Furthermore, mesostructured ribbons can also be obtained from the syntheses with hexadecyltrimethylammonium chloride (C_{16}TMAC), hexadecyltrimethylammonium bromide (C_{16}TMAB), and hexadecylpyridinium chloride (C_{16}PC) surfactants. The reaction compositions using C_{16}TMAC, C_{16}TMAB, and C_{16}PC for producing mesostructured ribbons are 100 H_2O:1.5–2.5 HCl:0.02 C_{16}TMAC:0.03 TEOS, 100 H_2O:1.5–2.5 HCl:0.02 C_{16}TMAB:0.03 TEOS, and 100 H_2O:2.0–3.5 HCl:0.02 C_{16}PC:0.03 TEOS, respectively. In contrast, ribbons were not obtained from syntheses that involved trimethylammonium surfactants with dodecyl, tetradecyl, or octadecyl hydrophobic tails. Low-angle XRD patterns with a step of 0.02° and time-per-step of 2 s were obtained on a Scintag PADX diffractometer by using Cu K_α radiation. SEM studies were performed on a JEOL 6340F microscope operating at 2–5 keV. TEM studies were carried out on a JEOL 2010 microscope operating at 200 keV. Silica ribbon samples were dispersed into ethanol and then deposited onto either silicon wafers or copper grids coated with carbon-stabilized lacey formvar for SEM or TEM imaging, respectively. To obtain cross-sectional TEM images, ribbon samples were embedded into a thermocurable resin (Eponate 12 kit, Ted Pella) and kept at 60 °C overnight. The embedded ribbon samples were then microtomed into thin slices of around 70 nm thickness, which were transferred onto bare copper grids for TEM observations. Nitrogen adsorption and desorption isotherms were measured using a Micromeritics TriStar 3000 system at liquid nitrogen temperature (−196 °C) after the samples were degassed with flowing nitrogen at 200 °C overnight.

Received: July 13, 2004

Keywords: cooperative effects · mesoporous materials · silicates · surfactants · template synthesis

[1] M. E. Davis, *Nature* **2002**, *417*, 813 – 821.
[2] a) Y. F. Lu, H. Y. Fan, A. Stump, T. L. Ward, T. Rieker, C. J. Brinker, *Nature* **1999**, *398*, 223 – 226; b) C. E. Fowler, D. Khushalani, B. Lebeau, S. Mann, *Adv. Mater.* **2001**, *13*, 649 – 652.
[3] H. Yang, N. Coombs, G. A. Ozin, *Nature* **1997**, *386*, 692 – 695.
[4] a) Q. S. Huo, D. Y. Zhao, J. L. Feng, K. Weston, S. K. Buratto, G. D. Stucky, S. Schacht, F. Schüth, *Adv. Mater.* **1997**, *9*, 974 – 978; b) F. Marlow, B. Spliethoff, B. Tesche, D. Y. Zhao, *Adv. Mater.* **2000**, *12*, 961 – 965; c) F. Kleitz, F. Marlow, G. D. Stucky, F. Schüth, *Chem. Mater.* **2001**, *13*, 3587 – 3595.
[5] Z. L. Yang, Z. W. Niu, X. Y. Cao, Z. Z. Yang, Y. F. Lu, Z. B. Hu, C. C. Han, *Angew. Chem.* **2003**, *115*, 4333 – 4335; *Angew. Chem. Int. Ed.* **2003**, *42*, 4201 – 4203.
[6] J. F. Wang, J. P. Zhang, B. Y. Asoo, G. D. Stucky, *J. Am. Chem. Soc.* **2003**, *125*, 13966 – 13967.
[7] H.-P. Lin, C.-Y. Mou, *Science* **1996**, *273*, 765 – 768.
[8] a) H. Yang, N. Coombs, I. Sokolov, G. A. Ozin, *Nature* **1996**, *381*, 589 – 592; b) Y. F. Lu, R. Ganguli, C. A. Drewien, M. T. Anderson, C. J. Brinker, W. L. Gong, Y. X. Guo, H. Soyez, B. Dunn, M. H. Huang, J. I. Zink, *Nature* **1997**, *389*, 364 – 368.
[9] a) S. Park, J.-H. Lim, S.-W. Chung, C. A. Mirkin, *Science* **2004**, *303*, 348 – 351; b) H. Y. Fan, K. Yang, D. M. Boye, T. Sigmon, K. J. Malloy, H. F. Xu, G. P. López, C. J. Brinker, *Science* **2004**, *304*, 567 – 571; c) J. F. Wang, G. D. Stucky, *Adv. Funct. Mater.* **2004**, *14*, 409 – 415.
[10] Z. P. Liu, S. Li, Y. Yang, S. Peng, Z. K. Hu, Y. T. Qian, *Adv. Mater.* **2003**, *15*, 1946 – 1948.
[11] a) Z. W. Pan, Z. R. Dai, Z. L. Wang, *Science* **2001**, *291*, 1947 – 1949; b) X. Y. Kong, Z. L. Wang, *Nano Lett.* **2003**, *3*, 1625 – 1631; c) X. Y. Kong, Y. Ding, R. Yang, Z. L. Wang, *Science* **2004**, *303*, 1348 – 1351; d) J. G. Yu, J. C. Yu, W. K. Ho, L. Wu, X. C. Wang, *J. Am. Chem. Soc.* **2004**, *126*, 3422 – 3423; e) M. Law, D. J. Sirbuly, J. C. Johnson, J. Goldberger, R. J. Saykally, P. D. Yang, *Science* **2004**, *305*, 1269 – 1273.
[12] C. Ma, Y. Ding, D. Moore, X. D. Wang, Z. L. Wang, *J. Am. Chem. Soc.* **2004**, *126*, 708 – 709.
[13] A. M. Seddon, H. M. Patel, S. L. Burkett, S. Mann, *Angew. Chem.* **2002**, *114*, 3114 – 3117; *Angew. Chem. Int. Ed.* **2002**, *41*, 2988 – 2991.
[14] G. Larsen, S. Noriega, R. Spretz, R. Velarde-Ortiz, *J. Mater. Chem.* **2004**, *14*, 2372 – 2373.
[15] S. Schacht, Q. Huo, I. G. Voigt-Martin, G. D. Stucky, F. Schüth, *Science* **1996**, *273*, 768 – 771.
[16] G. C. L. Wong, J. X. Tang, A. Lin, Y. L. Li, P. A. Janmey, C. R. Safinya, *Science* **2000**, *288*, 2035 – 2039.

